Microchim Acta (2016) 183:35–47
DOI 10.1007/s00604-015-1585-6

ORIGINAL PAPER

Multi-walled carbon nanotubes doped with boron as an electrode material for electrochemical studies on dopamine, uric acid, and ascorbic acid

Nikos G. Tsierkezos[1] · Uwe Ritter[1] · Yudi Nugraha Thaha[1] · Clive Downing[3] · Paweł Szroeder[2] · Peter Scharff[1]

Received: 17 July 2015 / Accepted: 25 July 2015 / Published online: 6 August 2015

Abstract Boron-doped multi-walled carbon nanotubes (B-MWCNTs) were deposited on oxidized silicon substrate via decomposition of ethanol and boric acid in the presence of the catalyst ferrocene by means of chemical vapor deposition in a thickness of typically 900 nm. The B-MWCNTs were characterized using Raman spectroscopy and scanning electron microscopy and transmission electron microscopy in combination with energy dispersive X-ray spectroscopy. The deposited B-MWCNTs were electrochemically characterized using the ferrocyanide/ferricyanide redox system by means of cyclic voltammetry and electrochemical impedance spectroscopy. The response of B-MWCNTs towards oxidation of dopamine (DA), uric acid (UA), and ascorbic acid (AA) was studied. DA, UA and AA can be determined at working potentials of typically 0.267, 0.412, and 0.127 V (vs. Ag/AgCl) with detection limits of 0.11, 0.65, and 1.21 μM, respectively.

Electronic supplementary material The online version of this article (doi:10.1007/s00604-015-1585-6) contains supplementary material, which is available to authorized users.

✉ Nikos G. Tsierkezos
nikos.tsierkezos@tu-ilmenau.de

[1] Department of Chemistry, Institute of Chemistry and Biotechnology Ilmenau University of Technology, Weimarer Straße 25, 98693 Ilmenau, Germany

[2] Institute of Physics, Faculty of Physics, Astronomy and Informatics, Nicolaus Copernicus University, Grudziadzka 5, 87-100 Toruń, Poland

[3] Advanced Microscopy Laboratory, CRANN, Trinity College Dublin, Dublin 2, Ireland

Keywords Ascorbic acid · Boron-doped carbon nanotubes · Dopamine · Electrochemical sensing · Raman spectroscopy · Transmission electron microscopy · Uric acid

Introduction

Multi-walled carbon nanotubes (MWCNTs) were widely used in electroanalysis due to their marvellous electrical, chemical, and mechanical properties [1]. MWCNTs were extensively used for fabrication of electrodes and electrochemical devices because they can improve the response and sensitivity of sensors due to their large surface area and their high electrical conductivity [2]. In addition, MWCNTs are considered as promising materials for future nanoelectronics and field-emission displays since their application as conducting or electron emitting devices improves their performance and simultaneously reduces significantly their size. Thus, considerable efforts were made to precisely control and enhance the conductivity of MWCNTs for such applications [3]. The conductivity of MWCNTs depends on their intrinsic structure, chirality, defects, and tube conformation that are directly related to the fabrication process. In addition, the electronic properties of MWCNTs are strongly connected to their delocalised electron system, and thus, the chemical modification of MWCNTs influences their electronic properties. Consequently, with the proper choice of type of modification, the electronic properties of MWCNTs can be purposely adjusted. The unique morphology of MWCNTs permits their modification, with wide variety of possible approaches, and thereby the variation of their physical and electronic properties. For instance, the possibility of attaching functional groups to the carbon nanotube surface allows the combination of properties of nanotubes and attached group. Currently, oxygen-containing functional groups, such as carboxylic, carbonyl,

and hydroxy groups that are usually obtained by chemical oxidation of nanotubes are widely used to enhance the surface energy and facilitate the binding sites [4]. Unfortunately, the oxygen-functional groups starkly worsen the electrical properties, the thermal/mechanical stability, and the carrier mobility of MWCNTs since such functionalization leads to defects that reduce the crystallinity and electrical conductivity of MWCNTs [5].

The doping of MWCNTs with heteroatoms became the main focus in recent MWCNTs research, since it leads to powerful controllability of electrical and chemical properties of MWCNTs [6]. Consequently, there is a great interest for developing new techniques for production of doped MWCNTs that incorporate into their structure heteroatoms, such as boron, phosphorus, or nitrogen to act as acceptors or electron donors. According to literature reports, the nitrogen-doping can effectively enhance the surface energy and reactivity of graphitic carbons with the minimum loss of material properties [7]. Besides, by controlling the chiral indices, the doping of nanotubes with boron can be attempted that results to lowering of Fermi level into the valence band [8, 9]. It was observed that the boron-doping improves the field emission properties, when compared to either pristine or nitrogen-doped MWCNTs, and thus increases the binding energies of carboxyl groups in carbon nanotubes [10, 11]. It is, therefore, not surprising that many scientists have already fabricated boron-doped nanotubes with decomposition of numerous boron source materials using various methods, such as catalytic pyrolysis, electric arc discharge, diffusion and solid state reaction, substitution and solid state reaction, spark plasma sintering, and laser vaporization (Table S1, ESM). However, among these methods, spray pyrolysis has the advantage of producing high yields of very clean boron-doped carbon nanotubes without amorphous carbon.

The present work reports on fabrication of boron-doped multi-walled carbon nanotubes (B-MWCNTs) onto silicon/silicon oxide substrate by means of chemical vapour deposition technique. The B-MWCNTs were fabricated using ethyl alcohol as carbon source material, boric acid as boron precursor, and ferrocene as catalyst. The B-MWCNTs were characterized using Raman spectroscopy as well as by means of scanning electron microscopy (SEM) and transmission electron microscopy (TEM) in combination with energy dispersive X-ray spectroscopy (EDX). The electrochemical characterization of B-MWCNTs was carried out using the standard redox system ferrocyanide/ferricyanide, $[Fe(CN)_6]^{3-/4-}$ in aqueous KCl solution (1.0 M) by means of cyclic voltammetry (CV) and electrochemical impedance spectroscopy (EIS) techniques. Furthermore, the electrochemical response of B-MWCNTs towards oxidation of dopamine (DA) and uric acid (UA) was carried out in phosphate buffer solution (pH 7.0). The interference of ascorbic acid (AA) in analysis of DA and UA was also probed.

Many publications dealing with carbon nanotubes-based sensors were already reported in literature. In those articles, the particular structure of carbon nanotubes and their unique properties that make them very attractive for the design of electrochemical biosensors were explored. For instance, an extensive review regarding the various electrochemical methods including numerous carbon-based composite films that can be applied for analysis of dopamine and other neurotransmitters was already reported by Sanghavi *et al*. [12]. In addition, a review article covering recent progress made on non-enzymatic electrochemical sensors that were widely used for determination of uric acid was recently reported by Chen *et al*. [13]. Furthermore, a review manuscript that summarizes the most relevant contributions in the last years in development of electrochemical sensors based on carbon nanotubes was reported by Rivas *et al*. [14]. In this article, the different strategies for constructing carbon nanotubes-based electrochemical sensors, their analytical performance, and future prospects were discussed. To the best of our knowledge, although many publications dealing with various types of doped carbon nanotubes appear in literature, carbon nanotubes doped with boron was not previously studied as electrode material in electrochemical sensing. Consequently, the present research work provides results on electrochemical analysis of fairly interesting biomolecules such as AA, DA, and UA onto B-MWCNTs.

Experimental

Materials and reagents

Boric acid (>99.5 %), ethyl alcohol (>99.5 %), ferrocene (>98.0 %), potassium hexacyanoferrate(III), (>99.0 %), potassium hexacyanoferrate(II) trihydrate, (>98.5 %), dopamine (>99.0 %), and potassium chloride (>99.0 %) were purchased from Sigma-Aldrich (www.sigmaaldrich.com), while L(+)-ascorbic acid (>99.7 %) and uric acid (>98.0 %) were purchased from Merck (www.merck.de) and Fluka (www.sigmaaldrich.com), respectively. All chemicals were used as received without any further purification. For electrochemistry measurements, a stock solution of $K_3Fe(CN)_6/K_4Fe(CN)_6$ binary mixture with concentration of 1.0×10^{-2} M was prepared by dissolving the appropriate amounts of salts in 1.0 M KCl aqueous solution. The stock solution of $[Fe(CN)_6]^{3-/4-}$ was prepared immediately prior the electrochemical experiments by using distilled water. The measured solutions of $[Fe(CN)_6]^{3-/4-}$ in the concentration range of 0.032–0.211 mM, were prepared directly in electrochemical cell with progressive addition of appropriate volume of stock solution in aqueous KCl solution (1.0 M). The solutions of DA, UA, and AA of

desired concentration were prepared immediately prior to measurements directly in electrochemical cell with addition of proper volumes of stock solutions of biomolecules into phosphate buffer solution (pH 7.0). The electrochemistry measurements were performed at pH 7.0 since this pH value is very close to the physiological pH (pH 7.365). Furthermore, it was verified that at pH 7.0 the voltammetric response of B-MWCNTs film towards oxidation of DA, UA, and AA is quite enhanced. The electrochemistry measurements were carried out at the room temperature.

Fabrication of B-MWCNTs

The growth of B-MWCNTs onto silicon/silicon oxide substrate was carried out successfully by means of chemical vapour deposition technique with decomposition of ethyl alcohol (carbon source material) and boric acid (boron source material) in the presence of ferrocene (catalyst). For the spray pyrolysis process, boric acid dissolved in absolute ethyl alcohol containing ferrocene (1.0 wt.%) was used. The concentration of boric acid was fixed at 1.0 wt.%, since high quality carbon nanotubes were obtained using such experimental conditions. For the growth process, the boric acid/ethyl alcohol/ferrocene ternary mixture was introduced to the furnace at the temperature of 850 °C through a syringe with flow rate of 0.17 mL min^{-1}. The growth processing time was fixed at about 30 min, and thus, a total volume of 5 mL of boric acid/ethyl alcohol/ferrocene ternary mixture was sprayed into furnace for the production of B-MWCNTs. It must be mentioned that less amount of sprayed solution (ca. 3 mL) leads to B-MWCNTs of lower quality. The B-MWCNTs-based films used as working electrodes for electrochemistry measurements were prepared according to following procedure: the fabricated B-MWCNTs films were initially connected to platinum wire by using silver conducting coating, and once the silver coating was dried, the silver conducting part of B-MWCNTs films was fully covered with varnish protective coating.

Instrumentations

The electrochemical measurements were carried out on electrochemical working station Zahner (IM6/6EX, Germany) (www.zahner.de) and the obtained data were analyzed by means of Thales software (version 4.15). A three electrode system consisting of B-MWCNTs-based working electrode, platinum plate counter electrode, and silver/silver chloride (saturated KCl) reference electrode was used for the electrochemistry measurements. The electrochemical impedance spectra were recorded in the frequency range from 0.1 Hz to 100 kHz at the half-wave potential of studied redox system $[Fe(CN)_6]^{3-/4-}$ ($E_{1/2}$=+0.270 V vs. Ag/AgCl). All electrochemistry measurements were carried out at the room temperature. All solutions were deoxygenated by purging with high-purity nitrogen for at least 10 m prior to measurements. The morphology and elemental composition of B-MWCNTs were examined by transmission electron microscope, TEM (FEI Titan operating at 300kv, images acquired using TEM and elemental analysis aquired using STEM) (www.fei.com), and scanning electron microscope, SEM (Zeiss Ultra with an Oxford instruments EDX detector) equipped with an energy dispersive X-ray spectrometer, EDX (www.zeiss.com). Raman spectra of B-MWCNTs were acquired with a inVia microprobe spectrometer (Renishow, Gloucestershire, UK) (www.renishaw.com), which was coupled to a Leica confocal microscope. A Laser excitation light of the length of 488 nm (2.54 eV) was used. Main Raman features characteristic to sp^2-carbon materials were fitted using Lorentzian curves.

Results and discussion

SEM/EDX and TEM analysis

Representative SEM and TEM images of fabricated B-MWCNTs composite film are shown in Fig. 1 and Fig. S1 (ESM), respectively. Furthermore, representative EDX spectra recorded for B-MWCNTs film are shown in Figs. S2-S5 (ESM). The SEM micrographs (Fig. 1) exhibit the presence of quite straight bundle of carbon nanotubes, which are obviously shorter compared to undoped pristine MWCNTs. Namely, well-aligned tiny B-MWCNTs, which are distributed homogenously onto the surface of silicon/silicon oxide substrate, were observed. The SEM images show that the samples are quite clean and almost free of amorphous carbon. The upper part of the B-MWCNTs holds cyclical-like structure with diameter in the range of 100–150 nm, while the side-walls of B-MWCNTs possess defects from which additional B-MWCNTs can be grown. Consequently, great amount of aligned B-MWCNTs possess the so-called “Y-shape” structure. Such behaviour was someway expected, since according to previous literature reports, the growing of carbon nanotubes in the presence of boron source materials results to defects along the axis of nanotubes [15]. Specifically, the modification of carbon nanotube’s structure with boron reduces the local hexagonal symmetry resulting therefore to defects in the structure of nanotubes. In addition, onto the surface of B-MWCNTs film numerous nanoadducts (nanoclusters) consisting of numerous B-MWCNTs having a so-called “star-shaped” form and possessing diameter in the range of 400–900 nm, can be also recognized in SEM images.

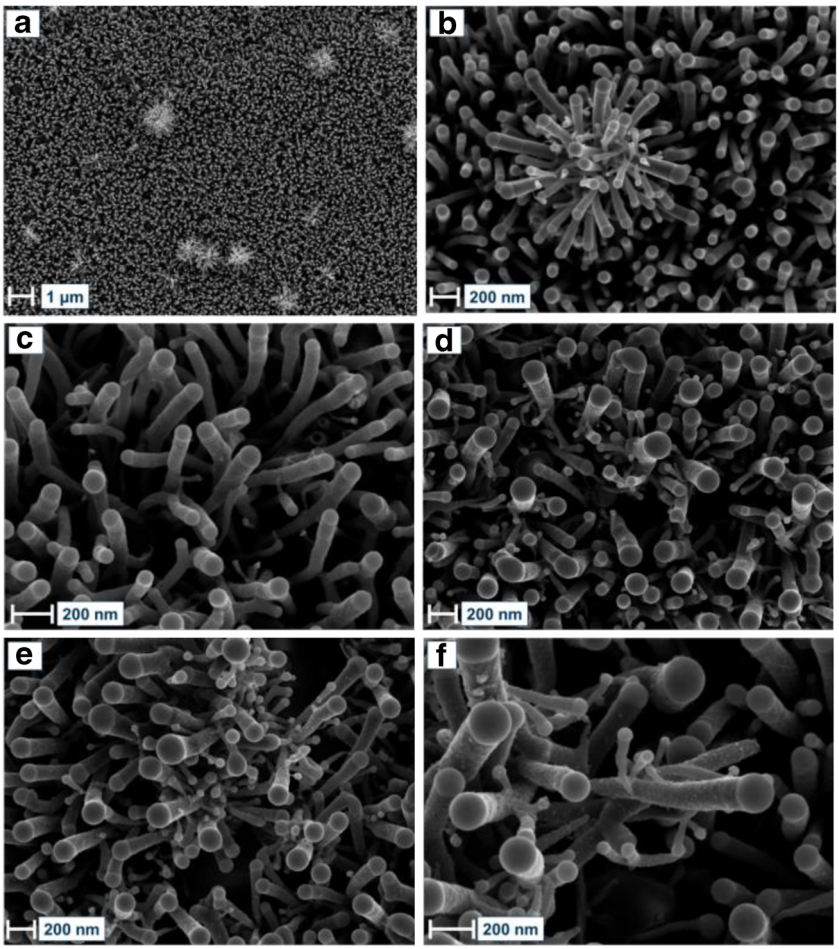

Fig. 1 SEM micrographs of B-MWCNTs composite film taken with accelerating voltage of 3.0 kV and magnification factors in the range of 5.0×10^3-6.0×10^4

The TEM micrographs (Fig. S1, ESM) reveal that the B-MWCNTs possess either cylinder-shaped or cone-shaped structure. In addition, the B-MWCNTs seem to be significantly shorter compared to either pristine MWCNTs or other types of MWCNTs (phosphorus-doped nanotubes, P-MWCNTs; nitrogen-doped nanotubes, N-MWCNTs) and possess uniform distribution in length and diameter. Besides, the B-MWCNTs appear to have smaller diameter compared to pristine MWCNTs. Specifically, according to TEM images, the length of B-MWCNTs lies in the range from 800 to 900 nm, while their inner and outer diameter was estimated at 30 and 50 nm, respectively.

The EDX spectra recorded by means of EDX system attached to SEM instrument (Figs. S2-S5, ESM) clearly show the presence of boron in the samples along with carbon, oxygen, and iron (catalysts residue). We have to mention that from EDX analysis copper, which arises from the sample support grid of TEM, was also identified. According to EDX analysis the upper- and inner-part of B-MWCNTs seem to be highly boron doped, while the walls of nanotubes consist exclusively of carbon. It is very interesting to mention that boron is detected always along with oxygen indicating that the upper- and inner-part of nanotubes is consisting mostly of boron oxide nanoparticles. The presence of iron nanoparticles at the tips and inside the tubes was also recognized. In this point we have to remark that, it is probable that some small amounts of boron, which are incorporated into the structure of nanotubes, cannot be detected by means of EDX, since the detector is not adequately sensitive for boron element.

Raman spectroscopy

In Fig. 2a, Raman spectra recorded for B-MWCNTs (p-type dopant) are compared with those recorded for P-MWCNTs, N-MWCNTs (n-type dopants), and pristine MWCNTs. The parameters of the main Raman features are presented in Table 1. Three Raman modes, G, G' and D, which are common features of majority of the sp^2-bonded carbon systems can be clearly seen in the samples probed. Additionally, the combination mode D+G in B-MWCNTs that appears at ~2920 cm^{-1} indicates large amount of defects on this particular film as a consequence of boron atoms that substitute the carbon atoms, as well as some topological defects. The I_D/I_G intensity ratio of the B-MWCNTs was found to be almost twice

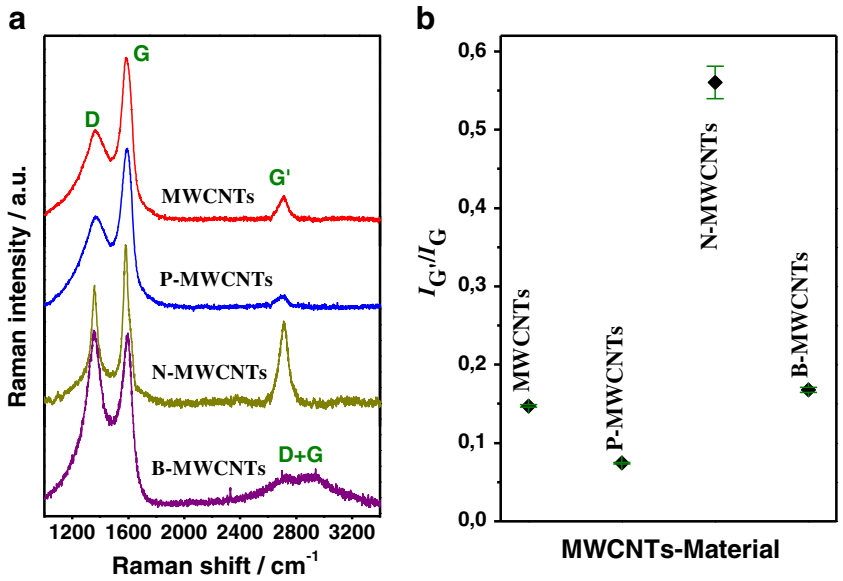

Fig. 2 **a** Raman spectra of pristine MWCNTs, P-MWCNTs, N-MWCNTs, and B-MWCNTs composite films; **b** Influence of acceptor doping on the blue shift of the G band

as large as in the pristine MWCNTs. Using the procedure described in literature [16] the average distance between defects in the B-MWCNTs was estimated to 9.1 nm. Slight upshift of the G-line is observed in the B-MWCNTs and the P-MWCNTs with respect to the undoped tubules. The blue shift of the G-line indicates that boron and phosphorus atoms substitute carbon atoms in tubule walls inject holes and electrons into the valence and conduction band of nanotubes, respectively. When the energy of creation of the electron–hole pair is less than energy of the G-band (about 0.2 eV), electron–phonon interaction between phonons and electrons near the Fermi level leads to the phonon hardening [17]. On the other hand, significant downshift of the G-line is observed in the N-MWCNTs. The strong red-shift of the G-band cannot be explained by donor doping and there should be other mechanisms responsible for such behavior, such as tensile strain [18]. The difference in the behavior of the N-MWCNTs and P-MWCNTs is probably also due to the properties of phosphorus- and nitrogen-doping states. The substitution of carbon atoms by nitrogen atoms create additional band lying beneath the conduction band, causing the N-MWCNTs to become metallic. On the other hand, the phosphorus doping states are strongly localized and do not contribute to the conductivity of the carbon nanotubes [19]. This finding is confirmed by the comparison of the $I_{G'}/I_G$ ratio, which depends strongly on the charge carrier concentration (Fig. 2b) [20]. The highest value of the $I_{G'}/I_G$ ratio is observed for N-MWCNTs. In the pristine MWCNTs and B-MWCNTs the $I_{G'}/I_G$ values was found to be intermediate, whereas the lowest value of the $I_{G'}/I_G$ is observed for P-MWCNTs.

Electrochemical response of B-MWCNTs towards $[Fe(CN)_6]^{3-/4-}$ redox system

Representative CVs recorded for $[Fe(CN)_6]^{3-/4-}$ (1.0 M KCl) on B-MWCNTs composite film at the scan rate of 0.02 $V \cdot s^{-1}$

Table 1 Positions of *D*, *G*, and *G*' Raman bands, and I_D/I_G and $I_{G'}/I_G$ ratios of pristine MWCNTs, P-MWCNTs, N-MWCNTs, and B-MWCNTs

Material	$\tilde{\nu}_D$ / cm^{-1}	$\tilde{\nu}_G$ / cm^{-1}	$\tilde{\nu}_{G'}$ / cm^{-1}	I_D/I_G	$I_{G'}/I_G$
MWCNTs[a]	1364.3±0.5	1588.14±0.15	2708±1	0.547±0.007	0.147±0.002
P-MWCNTs[b]	1366.4±0.5	1588.83±0.16	2697±2	0.580±0.008	0.074±0.001
N-MWCNTs[c]	1357.7±0.4	1584.01±0.18	2712.0±0.4	0.651±0.011	0.560±0.021
B-MWCNTs[d]	1357.6±0.4	1589.53±0.25	2728±18	1.038±0.020	0.168±0.003

[a] Pristine MWCNTs [21]

[b] Phosphorus-doped MWCNTs [21]

[c] Nitrogen-doped MWCNTs [21]

[d] Boron-doped MWCNTs (this work)

showing the effect of the change of concentration of redox system in the concentration range of 0.032–0.211 are shown in Fig. 3a. The change of the anodic current response of B-MWCNTs with the variation of the concentration of $[Fe(CN)_6]^{3-/4-}$ is presented graphically in Fig. 3b. The estimated electrochemical parameters obtained for various concentrations of $[Fe(CN)_6]^{3-/4-}$ on B-MWCNTs film are presented in Table S2 (ESM). As it can be seen in CVs shown in Fig. 3a, on B-MWCNTs a pair of well-defined reversible redox waves lying at about E_p^{ox}≈0.31 V (vs. Ag/AgCl) and E_p^{red}≈0.22 V (vs. Ag/AgCl) can be observed during the anodic and cathodic scans, respectively, corresponding to the one-electron transfer process involving the redox system $[Fe(CN)_6]^{3-/4-}$. The half-wave potential of $[Fe(CN)_6]^{3-/4-}$ on B-MWCNTs film, estimated as the average value of oxidation and reduction potentials, lies at about $E_{1/2}$≈0.270 V (vs. Ag/AgCl) and is almost similar within experimental error to that measured on either pristine MWCNTs ($E_{1/2}$≈0.271 V vs. Ag/AgCl), [21] P-MWCNTs ($E_{1/2}$≈0.271 V vs. Ag/AgCl), [21] and N-MWCNTs ($E_{1/2}$≈ 0.271 V vs. Ag/AgCl) [21] composite films. This finding confirms that the $E_{1/2}$ value for reversible redox systems is independent on working electrode's material. The recorded CVs illustrate that the investigated redox system $[Fe(CN)_6]^{3-/4-}$ appears to be reversible on B-MWCNTs film. Namely, the CVs recorded for $[Fe(CN)_6]^{3-/4-}$ on B-MWCNTs are quite symmetric and the peak current ratio of reverse and forward scans is equal to unity, and is independent of the scan rate. This behavior demonstrates that there are no parallel chemical reactions coupled to electrochemical process since such reactions would significantly alter the ratio of peak currents. Furthermore, the oxidative and reductive peak currents are essentially constant for several cycles. Namely, no loss of electro-activity was observed for recording continuously 50 cycles. This finding demonstrates that there are no chemical reactions coupled to electron transfer and that the involved electro-active species are stable in time frame of experiment confirming that the charge-transfer process occurring on B-MWCNTs film is reversible. It must be mentioned that similar behavior was observed for $[Fe(CN)_6]^{3-/4-}$ on pristine MWCNTs, P-MWCNTs, and N-MWCNTs films [21].

The effect of variation of scan rate on peak current of $[Fe(CN)_6]^{3-/4-}$ on B-MWCNTs film shows that the oxidation current varies linearly with the square root of scan rate indicating that the electrochemical process occurring on B-MWCNTs is diffusion controlled (Fig. S6, ESM). The last result is another evidence of the reversibility of investigated $[Fe(CN)_6]^{3-/4-}$ system on B-MWCNTs film. It must be mentioned that similarly the studied redox system $[Fe(CN)_6]^{3-/4-}$ appears to be diffusion controlled onto pristine MWCNTs, P-MWCNTs, and N-MWCNTs films [21].

The values of anodic and cathodic peak potential separation ($\Delta E_p = E_p^{ox} - E_p^{red}$) estimated for $[Fe(CN)_6]^{3-/4-}$ on B-MWCNTs film appear to be slightly dependent on concentration (ΔE_p increases slightly with concentration). Namely, the ΔE_p values vary from 0.077 to 0.121 V in the concentration range of 0.032–0.211 mM, and appear to be greater compared to ideal ΔE_p value of ΔE_p≈0.059 V that is indicative of reversible one-electron transfer redox process. It must be mentioned that the observed slight dependence of ΔE_p on concentration of redox system can be attributed to uncompensated resistance effect. Solak *et al*. [22] reported that the "observed" ΔE_p value for given redox system is the sum of "corrected" ΔE_p value and the term $2i_pR_u$, where i_p is either the oxidation or reduction peak current and R_u the uncompensated resistance of electrochemical cell. Consequently, the corrected ΔE_p value can be graphically estimated as intercept of the plot of "observed" ΔE_p *versus* i_p (with slope $2R_u$). As an example, the plot showing the variation of ΔE_p with the oxidation peak current of $[Fe(CN)_6]^{3-/4-}$ in concentration range of 0.032–0.211 mM on B-MWCNTs film is presented in Fig. S7a

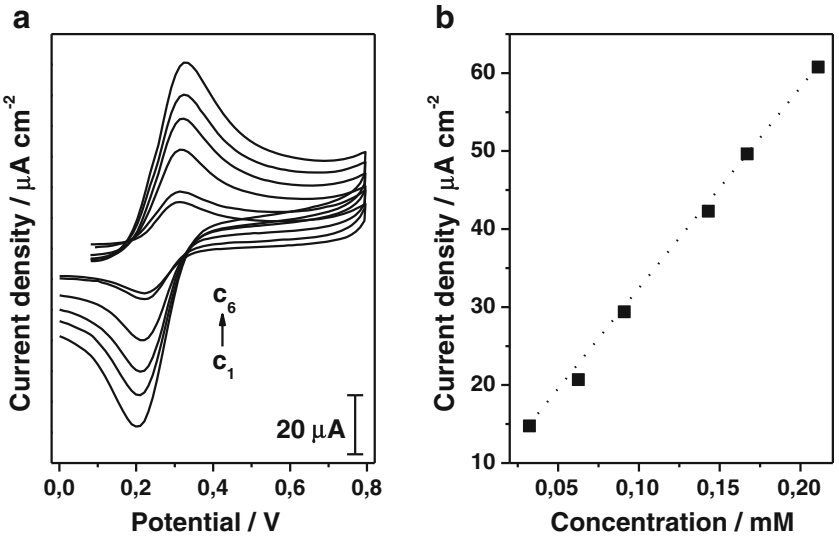

Fig. 3 **a** Representative CVs recorded for various concentrations of $[Fe(CN)_6]^{3-/4-}$ (1.0 M KCl) on B-MWCNTs composite film at the scan rate of 0.02 V·s^{-1}. The CVs from inner to outer correspond to concentrations: 0.032 mM (c_1), 0.062 mM (c_2), 0.091 mM (c_3), 0.143 mM (c_4), 0.167 mM (c_5), and 0.211 mM (c_6); **b** Effect of concentration on oxidation peak current density of $[Fe(CN)_6]^{3-/4-}$ (1.0 M KCl) on B-MWCNTs composite film

(ESM). The "corrected" ΔE_p values corresponding to "no effect" of concentration of electroactive species are presented graphically in Fig. S7b (ESM) and are also included in Table S2 (ESM) along with the "observed" ΔE_p values for comparison reasons. As it can be seen, the "corrected" ΔE_p values vary slightly with the concentration of redox system. Furthermore, the "corrected" ΔE_p values are very close (within experimental error) to theoretical ΔE_p value ($\Delta E_p \approx$ 0.059 V) indicating that the redox system is rather reversible onto B-MWCNTs. Besides, it can be clearly seen that the "corrected" ΔE_p values of $[Fe(CN)_6]^{3-/4-}$ on B-MWCNTs appear to be significantly smaller (18–46 %) compared to the corresponding "observed" ΔE_p values. Considering that the charge-transfer rate for redox system is estimated from the ΔE_p values by means of electrochemical absolute rate relation, this finding demonstrates the great incorrectness of kinetic parameters that would have resulted from the interpretation of "observed" ΔE_p values.

The heterogeneous electron transfer rate constant (k_s) values were estimated by means of electrochemical absolute rate relation that is based on degree of peak separation between the forward and reverse scans. Namely, in order to determine the heterogeneous electron transfer rate constants of $[Fe(CN)_6]^{3-/4-}$ on B-MWCNTs the procedure suggested by Nicholson [23] was applied, which relates k_s with the "corrected" ΔE_p through a working curve of dimensionless kinetic parameter ψ. The k_s values determined for various concentrations of $[Fe(CN)_6]^{3-/4-}$ (in the range of 0.032–0.211 mM) on B-MWCNTs film are included in Table S2 (ESM). As it can be seen in Table S2 (ESM), the k_s value changes only slightly with the concentration of $[Fe(CN)_6]^{3-/4-}$. For comparison reasons, the mean k_s value of $[Fe(CN)_6]^{3-/4-}$ on B-MWCNTs is reported in Table 2, along with the literature k_s values measured for the same redox system on pristine MWCNTs, P-MWCNTs, and N-MWCNTs films [21]. The findings demonstrate that the kinetics of redox process taking place onto B-MWCNTs film is more than two times faster (~130 % faster) compared to that occurring onto pristine MWCNTs. Furthermore, the charge-transfer kinetics of $[Fe(CN)_6]^{3-/4-}$ onto B-MWCNTs film appears to be slower (~22 % slower) compared to that taking place on N-MWCNTs, and faster (~40 % faster) compared to that occurring on P-MWCNTs. Specifically, as it can be seen in Table 2, the kinetic parameter k_s of $[Fe(CN)_6]^{3-/4-}$ on MWCNTs composite films tends to increase with the following order: pristine MWCNTs<P-MWCNTs<B-MWCNTs<N-MWCNTs. These findings exhibit that the doping of nanotubes with boron improves the kinetics of redox process occurring onto carbon nanotubes. However, according to these results, the doping of carbon nanotubes with boron oxide cannot compete the nitrogen-doping of nanotubes that improves even more the charge-transfer kinetics of the process occurring onto carbon nanotubes.

For estimating the detection ability and sensitivity of B-MWCNTs film towards $[Fe(CN)_6]^{3-/4-}$ the variation of oxidation peak current with the concentration of redox system was studied. The findings demonstrate that B-MWCNTs exhibits linear voltammetric response towards $[Fe(CN)_6]^{3-/4-}$ in the investigated concentration range of 0.032–0.211 mM (Fig. 3b). From the linear concentration-current curve the detection limit and sensitivity of B-MWCNTs towards $[Fe(CN)_6]^{3-/4-}$ were estimated to be 0.68 μM and 0.512 $A \cdot M^{-1} \cdot cm^{-2}$, respectively. It must be mentioned that the limit of detection was estimated for the concentration of $[Fe(CN)_6]^{3-/4-}$ that provides three times the ratio of analyte current to noise signal (S/N= 3). For comparison reasons, the detection limit and sensitivity of B-MWCNTs towards $[Fe(CN)_6]^{3-/4-}$ are included in Table 2 along with those reported in literature for pristine MWCNTs, P-MWCNTs, and N-MWCNTs films towards the same redox system [21]. As is can be recognized in Table 2, the detection limit of various types of MWCNTs towards $[Fe(CN)_6]^{3-/4-}$ tends to decrease with the following order: pristine MWCNTs>P-MWCNTs>B-MWCNTs>N-MWCNTs. Specifically, the detection ability of carbon nanotubes doped with boron appears to be about 57 and 32 % greater compared to that of pristine MWCNTs and P-MWCNTs, respectively,

Table 2 Half-wave potential ($E_{1/2}$), heterogeneous electron-transfer rate constant (k_s), charge-transfer resistance (R_{ct}), lower limit of detection (*LOD*), and sensitivity (*S*) for $[Fe(CN)_6]^{3-/4-}$ (1.0 M KCl) on pristine MWCNTs, P-MWCNTs, N-MWCNTs, and B-MWCNTs composite films

Parameter	MWCNTs[a]	P-MWCNTs[b]	N-MWCNTs[c]	B-MWCNTs[d]
$E_{1/2}$ / V	0.271	0.271	0.271	0.270
k_s / 10^{-3} $cm \cdot s^{-1}$	9	15	27	21
R_{ct} / Ω	50	35	17	23
LOD / μM	1.57	1.00	0.47	0.68
S / $A \cdot M^{-1} \cdot cm^{-2}$	0.423	0.499	0.540	0.512

[a] Pristine MWCNTs [21]

[b] Phosphorus-doped MWCNTs [21]

[c] Nitrogen-doped MWCNTs [21]

[d] Boron-doped MWCNTs (this work)

while their detection ability seems to be about 45 % poorer compared to that of N-MWCNTs. These findings confirm the particularly enhanced electrocatalytic activity of carbon nanotubes that incorporate nitrogen atoms into their structure. This behavior can be explained through the extra valence electrons of dopant material that occupy the carbon nanotubes conduction band and shift the Fermi level toward the conduction band improving the conductivity of nanotubes and enhancing their electrochemical response [24]. It is not surprising that the sensitivity of MWCNTs composite films towards $[Fe(CN)_6]^{3-/4-}$ tends likewise to increase with the order: pristine MWCNTs<P-MWCNTs<B-MWCNTs<N-MWCNTs (Table 2). It is very interesting that with the same order increases the kinetic parameter k_s of $[Fe(CN)_6]^{3-/4-}$, indicating that the modification of carbon nanotubes with phosphorus, boron, and nitrogen improves progressively their electrocatalytic properties.

It would be very interesting to compare the lower limit of detection of B-MWCNTs towards $[Fe(CN)_6]^{3-/4-}$ with those reported in literature for other electrodes. Perenlei *et al.* [25] reported that the detection limits of glassy carbon electrode modified with MWCNTs and titanium dioxide towards $[Fe(CN)_6]^{3-/4-}$ estimated at the scan rates of 0.10 $V \cdot s^{-1}$ and 0.005 $V \cdot s^{-1}$ are *LOD*=48.6 μM and *LOD*=1.10 μM, respectively. These literature *LOD* values appear to be poorer compared to that estimated in present work for B-MWCNTs film towards the same redox system at the scan rate of 0.02 $V \cdot s^{-1}$ (*LOD*=0.68 μM). Additionally, Pandurangachar *et al.* [26] reported that the detection limit of carbon paste electrode modified with 1-butyl 4-methylpyridinium tetrafluoro borate towards $[Fe(CN)_6]^{3-/4-}$ is about *LOD*=100 μM that is noticeably poorer compared to that estimated for B-MWCNTs towards the same redox system (*LOD*=0.68 μM). Besides, the detection limit of carbon paste electrode modified with sodium dodecyl sulphate towards $[Fe(CN)_6]^{3-/4-}$ of about *LOD*= 100 μM, reported by Niranjana *et al.*, [27] appears to be also significantly poorer compared to that obtained for B-MWCNTs towards $[Fe(CN)_6]^{3-/4-}$ (*LOD*=0.68 μM). In addition, Hirano *et al.* [28] reported that a glass capillary ultramicroelectrode has detection limit of *LOD*=30 μM towards $[Fe(CN)_6]^{3-/4-}$ that is also remarkably poorer compared to that estimated for B-MWCNTs towards $[Fe(CN)_6]^{3-/4-}$ (*LOD*= 0.68 μM). This comparison demonstrates that the detection ability of B-MWCNTs film appears to be significantly greater compared to other composite films reported in literature exhibiting the excellent electrocatalytic performance of B-MWCNTs film.

The electrochemical behavior of redox system $[Fe(CN)_6]^{3-/4-}$ on B-MWCNTs film was further investigated by means of EIS technique. A representative EIS spectrum, recorded for 0.211 mM $[Fe(CN)_6]^{3-/4-}$ (1.0 M KCl) on B-MWCNTs, is displayed in Fig. 4a. The EIS spectra recorded for various concentrations of $[Fe(CN)_6]^{3-/4-}$ (in the range of 0.032–0.211 mM) on B-MWCNTs are reported in Fig. S8 (ESM). In recorded EIS spectra, which are graphically displayed as Nyquist plots, the complex impedance of studied redox system is presented as the sum of real and imaginary impedance components. The type of recorded EIS spectra reveals that the impedance is controlled by interfacial electron transfer at high frequencies, while at low frequencies the Warburg impedance is generated. Namely, the EIS spectra at high frequencies include a part of small depressed semicircle that is almost invisible and corresponds to electron-transfer limiting process, and a linear part at middle and low frequencies that results from the diffusion limiting step of electrochemical process. These findings imply that the B-MWCNTs film exhibits in general great electrical conductivity or low internal resistance including polarization impedance. The absence of semicircle in complex impedance plane can be explained by means of high ionic conductivity at electrode/electrolyte interface and indicates the excellent electrochemical quality of B-MWCNTs film. It is interesting that in EIS spectra recorded for the same redox system on pristine MWCNTs a semicircle with large diameter can be recognized indicating that onto this particular film the charge-transfer process is the rate determining step. The recorded impedance spectra were satisfactorily fitted to the equivalent electrical circuit ($R_s+(C_{dl}/(R_{ct}+Z_w))$) (software Thales, version 4.15) (Fig. S9, ESM). The elements of electrical circuit are explained as follows: R_s is the Ohmic resistance of electrolyte, R_{ct} the charge-transfer resistance, C_{dl} the double-layer capacitance, and Z_w the Warburg diffusion impedance. The electrical circuit used was found to fit satisfactorily the impedance data over the entire investigated frequency range of 0.1 Hz-100 kHz. The mean and maximum modified impedance errors resulted from simulation process were estimated in all cases to be less than 0.2 and 4.0 %, respectively, which can be considered quite acceptable. In order to obtain satisfactory reproduction of experimental impedance data, the capacitor was replaced by constant phase element. The explanation for the presence of constant phase element is the microscopic roughness of surface of B-MWCNTs film that causes an inhomogeneous distribution in solution resistance and double-layer capacitance. The most suitable impedance parameter for further evaluation of electrochemical features and interfacial properties of B-MWCNTs film is the charge transfer resistance (R_{ct}). This impedance parameter is connected to charge-transfer kinetics of redox system at electrode interface and represents the barrier for electron-transfer process occurring onto electrode's surface. Specifically, R_{ct} represents the hindering behavior of interface properties of electrode and it can be estimated from diameter of capacitive semicircle that appears in Nyquist plots in the high-frequency region of EIS spectrum. The R_{ct} values estimated for various concentrations of $[Fe(CN)_6]^{3-/4-}$ on B-MWCNTs are included in Table S2 (ESM). In addition, the variation of R_{ct} with the concentration of $[Fe(CN)_6]^{3-/4-}$ in the range of

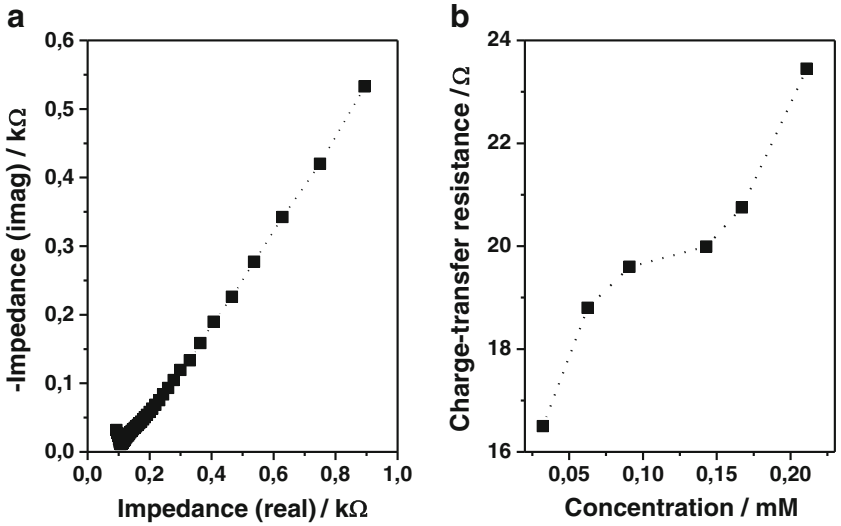

Fig. 4 **a** EIS recorded for 0.211 mM $[Fe(CN)_6]^{3-/4-}$ (1.0 M KCl) on B-MWCNTs composite film at the half-wave potential of studied redox system (+0.270 V vs. Ag/AgCl) in the frequency range of 0.1 Hz–100 kHz; **b** Effect of concentration on charge-transfer resistance of $[Fe(CN)_6]^{3-/4-}$ (1.0 M KCl) on B-MWCNTs composite film

0.032–0.211 mM is presented graphically in Fig. 4b. As it can be seen in Fig. 4b, the change of concentration of $[Fe(CN)_6]^{3-/4-}$ affects slightly the film's impedance behavior. Namely, the findings demonstrate that the charge-transfer resistance, and thus the barrier for electron-transfer, tends to increase marginally with rising concentration of $[Fe(CN)_6]^{3-/4-}$. This observation is probably connected to interruption of electron-transfer process caused by uncompensated resistance effect that becomes more significant with the increase of concentration of electroactive compound. The greatest R_{ct} value estimated for 0.211 mM $[Fe(CN)_6]^{3-/4-}$ on B-MWCNTs is included in Table 2 along with the R_{ct} values obtained for $[Fe(CN)_6]^{3-/4-}$ on pristine MWCNTs, P-MWCNTs, and N-MWCNTs for comparison reasons [21]. As it can be seen, the R_{ct} values, and consequently the barrier for electron transfer, tend to decrease with the following order: MWCNTs > P-MWCNTs > B-MWCNTs > N-MWCNTs. The results demonstrate that the modification of carbon nanotubes with various elements diminishes the barrier for electron transfer and improves the kinetic of redox process occurring on surface of carbon nanotubes. Nevertheless, within various different doping elements studied, nitrogen seems to improve better the electrocatalytic activity of carbon nanotubes. The impedance results are in absolute agreement with the kinetic parameter k_s achieved from CV data (Table 2). Namely, the k_s value of $[Fe(CN)_6]^{3-/4-}$ on pristine and various modified MWCNTs tends to increase with the order: MWCNTs < P-MWCNTs < B-MWCNTs < N-MWCNTs, confirming that the charge-transfer resistance is inversely proportional to exchange current, and thus, to heterogeneous electron-transfer rate constant. Furthermore, it is very interesting that with the same order, the detection capability of pristine and doped MWCNTs films towards $[Fe(CN)_6]^{3-/4-}$ tends to increase, demonstrating that the diminishing of barrier for electron transfer leads to an improvement of electrode's detection ability.

For better interpretation of the variation of electrochemical parameters of pristine and various doped-MWCNTs, the charge-transfer resistance, the rate of electron transfer, the lower limit of detection, and the sensitivity of MWCNTs films towards $[Fe(CN)_6]^{3-/4-}$ are presented graphically in histograms shown in Fig. 5. From these histograms, it can be clearly seen that within the films fabricated, the N-MWCNTs film possesses the smallest charge-transfer resistance, the greatest rate for electron transfer, the lowest limit of detection, and thus the highest sensitivity towards $[Fe(CN)_6]^{3-/4-}$. In addition, among the films tested, the pristine MWCNTs film reveals the slowest charge-transfer kinetic, the greatest barrier for electron transfer, and consequently the lowest detection ability. The B-MWCNTs composite film produced in present work lies electrochemically within N-MWCNTs and P-MWCNTs.

Application of B-MWCNTs in electrochemical sensing of AA

The response of B-MWCNTs film towards oxidation of molecules with biological interest, such as DA and UA was tested in phosphate buffer solution at pH 7.0. The influence of AA as interfering material was additionally studied since high doses of AA can interfere with the electrochemical analysis of DA and UA. Representative CVs recorded for AA, DA, and UA (phosphate buffer solution, pH 7.0) on B-MWCNTs are shown in Fig. 6a. As it can be seen in CV shown in Fig. 6a the irreversible oxidation of AA onto B-MWCNTs occurs at about +0.127 V (vs. Ag/AgCl). It is well known that AA can be electrochemically oxidized to dehydro-L-ascorbic acid [29]. The findings demonstrate that the ability of B-MWCNTs to diminish the overpotential of AA is comparable to that of N-MWCNTs and greater compared to P-MWCNTs

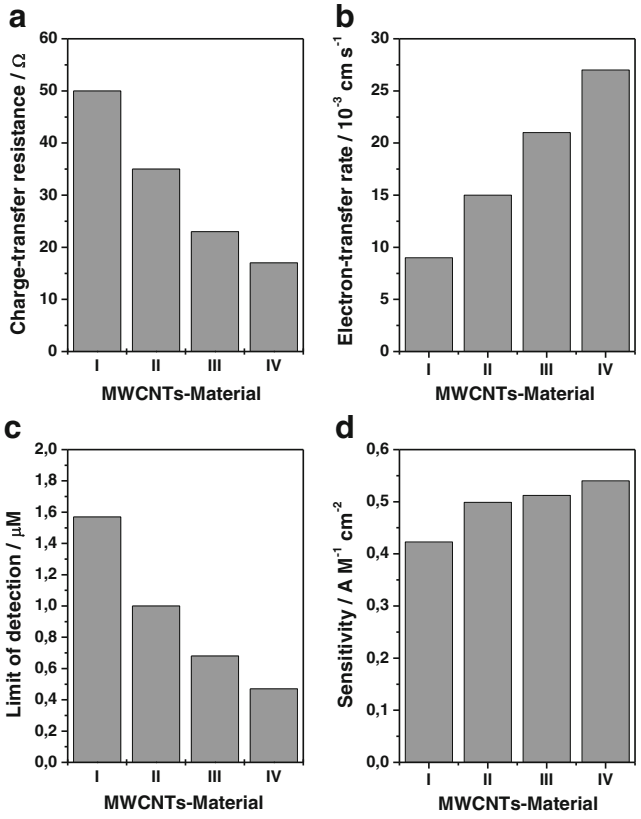

Fig. 5 Histograms showing the charge-transfer resistance **a**, the electron-transfer rate constant **b**, the lower limit of detection **c**, and the sensitivity **d** obtained for $[Fe(CN)_6]^{3-/4-}$ (1.0 M KCl) of pristine MWCNTs (I) [21], P-MWCNTs (II) [21], B-MWCNTs (III), and N-MWCNTs (IV) [21] composite films

and pristine MWCNTs. Specifically, the oxidation overpotential of AA onto B-MWCNTs (+0.127 V vs. Ag/AgCl) appears to be about 5 mV more anodic (positive) compared to that measured onto N-MWCNTs (+0.122 V vs. Ag/AgCl) [30]. Furthermore, the oxidation potential of AA on B-MWCNTs (+0.127 V vs. Ag/AgCl) seems to be about 221 and 259 mV less anodic (positive) compared to that measured onto P-MWCNTs (+0.348 V vs. Ag/AgCl) [31] and pristine MWCNTs (+0.386 V vs. Ag/AgCl), [30] respectively. These findings demonstrate the tendency of carbon nanotubes doped with boron to lower the overpotential of AA. From CVs shown in Fig. 6a it can be observed that the response of B-MWCNTs towards oxidation of AA is somehow restricted. Namely, it can be seen that for the same concentration of biomolecules the peak current response of B-MWCNTs towards oxidation of AA appears to be significantly lesser (more than 40 % lesser) compared to that for DA and UA. Thus, the lower limit of detection of B-MWCNTs towards oxidation of AA estimated at about 1.21 μM appears to be significantly poorer compared to those of DA and UA (see next paragraphs).

Application of B-MWCNTs in electrochemical sensing of DA

In CV shown in Fig. 6a it can be seen that the irreversible oxidation peak of DA onto B-MWCNTs occurs at about +0.267 V (vs. Ag/AgCl), which lies about 140 mV more anodic compared to oxidation peak of AA. As was already suggested, the oxidation of DA can be characterized as two-electron transfer process that leads to formation of dopamine-o-quinone [32]. In order to estimate the lower limit of detection of B-MWCNTs towards oxidation of DA, various concentrations of DA were measured in the range of 0.062–0.250 mM. Representative CVs recorded for various concentrations of DA on B-MWCNTs (phosphate buffer

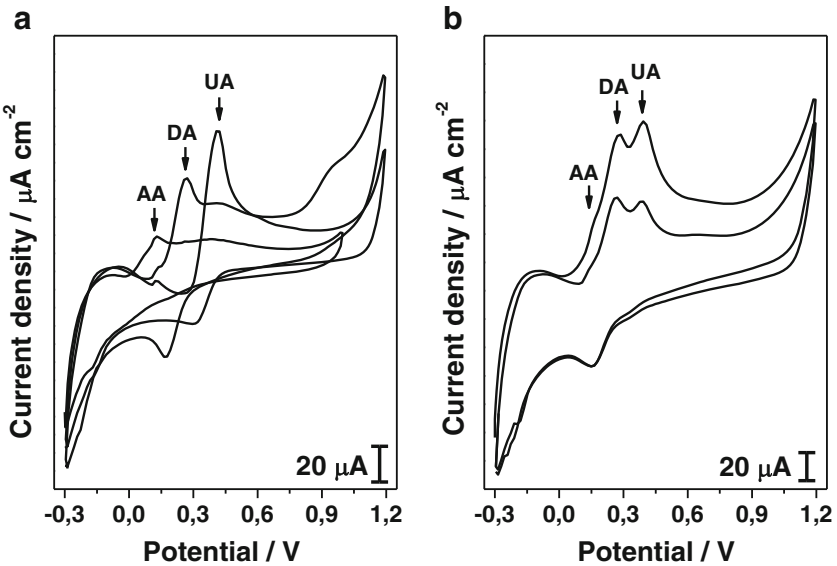

Fig. 6 **a** CVs recorded for AA (0.250 mM), DA (0.250 mM), and UA (0.250 mM) on B-MWCNTs composite film at the scan rate of 0.02 $V \cdot s^{-1}$ (phosphate buffer solution, pH 7.0); **b** CVs recorded for AA/DA/UA ternary mixtures on B-MWCNTs composite film at the scan rate of 0.02 $V \cdot s^{-1}$ (phosphate buffer solution, pH 7.0). The CVs from inner to outer correspond to AA/DA/UA ratios of 1:1:1 and 2:1:1

solution, pH 7.0) at the scan rate of 0.02 $V \cdot s^{-1}$ are shown in Fig. S10a (ESM). From the linear variation of oxidation peak current of DA with the concentration (Fig. S11a, ESM), the detection limit of B-MWCNTs towards oxidation of DA was estimated to be 0.11 μM. The limit of detection of B-MWCNTs towards DA appears to be about 11 times lower (better) compared to that obtained for the same composite film towards AA.

Application of B-MWCNTs in electrochemical sensing of UA

The CV recorded for UA reveals that the irreversible oxidation peak of UA onto B-MWCNTs appears at about +0.412 V (vs. Ag/AgCl) (Fig. 6a) that lies about 285 and 145 mV more anodic (positive) compared to oxidation peaks of AA and DA, respectively. Previous published studies suggested that the oxidation peak can be attributed to primary two electron oxidation of UA to uric acid diimine [33]. It is remarkable that the oxidation peak separation between AA-DA and DA-UA couples is nearly the same (about 140 mV). In order to estimate the lower limit of detection of B-MWCNTs towards oxidation of UA various concentrations of UA in range of 0.062–0.250 mM were measured. Representative CVs recorded for various concentrations of UA on B-MWCNTs (phosphate buffer solution, pH 7.0) at the scan rate of 0.02 $V\ s^{-1}$ are shown in Fig. S10b (ESM). From the linear variation of oxidation peak current of UA with the concentration (Fig. S11b, ESM), the detection limit of B-MWCNTs towards oxidation of UA was estimated to be 0.65 μM. The findings demonstrate that the limit of detection of B-MWCNTS towards oxidation of UA appears to be about 6 times greater compared to that obtained for DA and about 2 times lower compared to that measured for AA.

Application of B-MWCNTs in electrochemical sensing of AA, DA, and UA

The narrow response of B-MWCNTs towards AA and the diminishing of its oxidation overpotential on this particular film do not minimize the strong interference of AA in simultaneous voltammetric analysis with DA and UA. Consequently, in CVs recorded for AA/DA/UA ternary mixtures the redox waves of AA and DA overlap each other hindering, thus, their simultaneous analysis (Fig. 6b). The findings exhibit that the AA oxidation wave interferes with DA and likewise the oxidation wave of DA hinders the analysis of AA. We have to mention that analogous results were obtained on N-MWCNTs composite film [30]. Nevertheless, the AA/UA and DA/UA binary systems can be simultaneously analyzed on B-MWCNTs composite film since their electrochemical waves do not overlap each other. Specifically, in CVs recorded for AA/UA (1:1) and DA/UA (1:1) binary systems well-separated oxidation waves were recognized with peak potential separations of 280 and 144 mV, respectively that permit their simultaneous analysis in single measurement (Fig. 7). It is interesting that well separated redox waves can be still observed in AA/UA and DA/UA binary systems even if the concentration of AA and DA is 10 times higher compared to that UA (Fig. 7). However, with further increase of concentration of AA and DA up to 100 times higher compared to that of UA, an overlapping of oxidation peaks of biomolecules occurs hindering therefore their simultaneous analysis in single measurement. As an example, CVs recorded for various ratios of

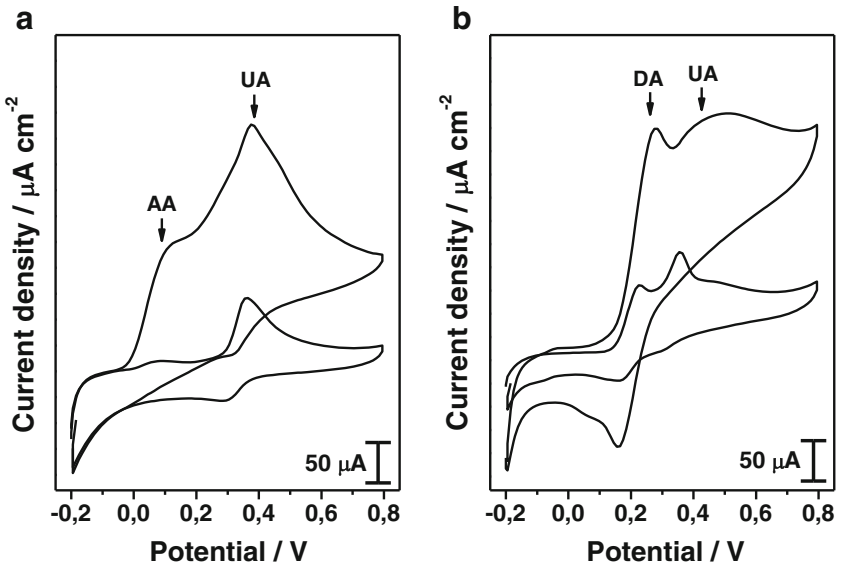

Fig. 7 CVs recorded for AA/UA **a** and DA/UA **b** binary mixtures on B-MWCNTs composite film at the scan rate of 0.02 $V \cdot s^{-1}$ (phosphate buffer solution, pH 7.0). The CVs from inner to outer correspond to AA/UA and DA/UA ratios of 1:1 and 10:1

AA/UA and DA/UA binary systems are shown in Figs. S12 and S13 (ESM), respectively.

The repeatability and reproducibility of B-MWCNTs were evaluated by means of CV technique. The reproducibility of the method was studied by measuring the electrochemical response of five different B-MWCNTs films towards oxidation of biomolecules. In all cases, reproducibility of less than 3.5 % was estimated. Furthermore, the repeatability of the method was studied by monitoring the current response of the same B-MWCNTs film towards oxidation of biomolecules for 10 different successive measurements. In all cases, repeatability of less than 3.2 % was estimated for B-MWCNTs that can be considered quite acceptable. The findings demonstrate that B-MWCNTs film has quite good repeatability and reproducibility towards the studied biomolecules.

For comparison reasons the detection limits for B-MWCNTs towards oxidation of DA, UA, and AA are reported along with those published in literature for pristine MWCNTs, P-MWCNTs, and N-MWCNTs films in Table 3. In addition, the limits of detection of pristine MWCNTs, P-MWCNTs, B-MWCNTs, and N-MWCNTs towards oxidation of DA and UA are presented graphically in histograms in Fig. S14 (ESM) [30, 31, 34, 35]. Furthermore, a comprehensive comparison of detection limits of B-MWCNTs and other composite films reported in literature towards oxidation of DA, UA, and AA is shown in Table S3 (ESM). From histograms shown in Fig. S14 (ESM) it can be clearly seen that the detection ability of carbon nanotubes doped with various elements towards oxidation of DA and UA tends to enhance with the following order: MWCNTs<P-MWCNTs<B-MWCNTs<N-MWCNTs. The results demonstrate that the doping of carbon nanotubes with boron improves the sensitivity of carbon nanotubes compared to either undoped nanotubes or phosphorus-doped nanotubes, but however the electrocatalytic properties of nitrogen-doped carbon nanotubes appear to be slightly more enhanced. Nevertheless, the B-MWCNTs composite film appears to be more sensitive compared to other films reported in literature (Table S3, ESM). It is very interesting that in some cases the detection ability of B-MWCNTs towards the studied redox systems appears to be ten times greater compared to other composite films. The findings demonstrate that B-MWCNTs is quite promising material for further applications in electrochemical sensing.

Table 3 Comparison of low limits of detection (*LOD*) (*S*/*N*=3) of pristine MWCNTs, P-MWCNTs, N-MWCNTs, and B-MWCNTs composite films towards oxidation of DA, UA, and AA (phosphate buffer solution, pH 7.0)

Electrodes	*LOD* / μM		
	DA	UA	AA
B-MWCNTs	0.11[a]	0.65[a]	1.21[a]
P-MWCNTs	0.19[b]	0.80[b]	1.12[b]
N-MWCNTs	0.03[c]	0.54[d]	0.97[d]
MWCNTs	0.30[e]	1.00[f]	8.00[f]

[a] Boron-doped MWCNTs (this work)

[b] Phosphorus-doped MWCNTs [31]

[c] Nitrogen-doped MWCNTs [34]

[d] Nitrogen-doped MWCNTs [30]

[e] Pristine MWCNTs [34]

[f] MWCNTs modified with iron(II) thiocyanate complex [35]

Conclusions

The presence research work reports on fabrication of B-MWCNTs on Si/SiO_2 substrate with decomposition of ethyl alcohol and boric acid in the presence of catalyst by means of spray pyrolysis. The B-MWCNTs were characterized using SEM/EDX and TEM as well as by means of Raman spectroscopy. SEM images show that B-MWCNTs are "Y-shaped" and their upper-part holds cyclical-like structure. TEM images reveal that the B-MWCNTs possess cylinder-shaped or cone-shaped structure and are smaller in length and diameter compared to pristine MWCNTs. EDX analysis demonstrate that the upper- and inner-part of nanotubes contains boron oxide nanoparticles, while the walls of nanotubes consist exclusively of carbon. Raman spectroscopy analysis exhibits that the ratio of D/G intensities is significantly greater in B-MWCNTs compared to pristine MWCNTs, P-MWCNTs, and N-MWCNTs. Electrochemical studies reveal that B-MWCNTs film is quite suitable for analysis of AA, DA, and UA with limits of detection at 1.21, 0.11, and 0.57 μM, respectively. The interference of AA in analysis of UA and DA was tested. The findings show that AA does not interfere with UA, but nevertheless considerable interference of AA in analysis of DA was recognized. B-MWCNTs appear to be more sensitive compared to other materials reported in literature and thus it can be considered as promising material for future applications in electrochemical sensing.

Acknowledgments The authors would like to thank Mrs. Doreen Schneider and Mrs. Sabine Heusing (Ilmenau University of Technology). The SEM/EDX and TEM/EDX analysis was carried out at Advanced Microscopy Laboratory (Trinity College Dublin, Ireland) with the financial support of European Commission (QualityNano; Grant Agreement No: FP7-262163; Application TCD-TAF-436). The authors would like to thank Mr. Colm McAtamney (CRANN, Trinity College Dublin, Ireland) for his supportive contributions to this work.

References

1. Bernholc J, Brenner D, Buongiorno Nardelli M, Meunier V, Roland C (2002) Mechanical and electrical properties of nanotubes. Annu Rev Mater Res 32:347
2. Musamech M, Wang J, Merkoci A, Lin Y (2002) Low-potential stable NADH detection at carbon-nanotube-modified glassy carbon electrodes. Electrochem Commun 4:743

3. Maultzsch J, Reich S, Thomsen C, Webster S, Czerw R, Carroll DL, Vieira SMC, Birkett PR, Rego CA (2002) Raman characterization of boron-doped multi-walled carbon nanotubes. Appl Phys Lett 81:2647
4. Balasubramanian K, Burghard M (2005) Chemically functionalized carbon nanotubes. Small 1:180
5. Peng H, Reverdy P, Khabashesku VN, Margrave JL (2003) Sidewall functionalization of single-walled carbon nanotubes with organic peroxides. Chem Commun 2003:362
6. Maiti UN, Lee WJ, Lee JM, Oh Y, Kim JY, Kim JE, Shim J, Han TH, Kim SO (2014) Chemically modified/doped carbon nanotubes and graphene for optimized nanostructures and nanodevices. Adv Mater 26:40
7. Lee DH, Lee WJ, Kim SO (2009) Highly efficient vertical growth of wall-number-selected N-doped carbon nanotube arrays. Nano Lett 9:1427
8. Ayala P, Arenal R, Loiseau A, Rubio A, Pichler T (2010) The physical and chemical properties of heteronanotubes. Rev Mod Phys 82:1843
9. Koretsune T, Saito S (2008) Electronic structure of boron-doped carbon nanotubes. Phys Rev B 77:165417
10. Sharma RB, Late DJ, Joag DS, Govindaraj A, Rao CNR (2006) Field emission properties of boron and nitrogen doped carbon nanotubes. Chem Phys Lett 428:102
11. Al-Aqtash N, Vasiliev I (2011) Ab initio study of boron- and nitrogen-doped graphene and carbon nanotubes functionalized with carboxyl groups. J Phys Chem C 115:18500
12. Sanghavi BJ, Wolfbeis OS, Hirsch T, Swami NS (2015) Nanomaterial-based electrochemical sensing of neurological drugs and neurotransmitters. Microchim Acta 182:1
13. Chen X, Wu G, Cai Z, Oyama M, Chen X (2014) Advances in enzyme-free electrochemical sensors for hydrogen peroxide, glucose, and uric acid. Microchim Acta 181:689
14. Rivas GA, Rubianes MD, Rodríguez MC, Ferreyra NF, Luque GL, Pedano ML, Miscoria SA, Parrado C (2007) Carbon nanotubes for electrochemical biosensing. Talanta 74:291
15. Handuja S, Srivastava P, Vankar VD (2009) Structural modification in carbon nanotubes by boron incorporation. Nanoscale Res Lett 4:789
16. Szroeder P, Górska A, Tsierkezos N, Ritter U, Strupiński W (2013) The role of band structure in electron transfer kinetics in low-dimensional carbon. Mat-wiss u Werkstofftech 44:226
17. Das A, Piana B, Chakraborty S, Piscanec S, Saha S, Waghmare U, Novoselov KS, Krishnamurthy HR, Geim AK, Ferrari AC, Sood AK (2008) Monitoring dopants by raman scattering in an electrochemistry top-gated graphene tranistor. Nat Nanotechnol 3:210
18. Ni ZH, Yu T, Lu YH, Wang YY, Feng YP, Shen ZX (2008) Uniaxial strain on graphene: raman spectroscopy study and band gap opening. ACS Nano 2:2301
19. Maciel IO, Campos-Delgado J, Cruz-Silva E, Pimenta MA, Sumpter BG, Meunier V, López-Urías F, Muñoz-Sandoval E, Terrones H, Terrones M, Jorio A (2009) Synthesis, electronic structure, and raman scattering of phosphorus-doped single-wall carbon nanotubes. Nano Lett 9:2267
20. Kuzmany H (2014) In: Tanaka K, Iijima S (eds) Phonon structures and raman effect of carbon nanotubes and graphene, 2nd edn. Elsevier, Amsterdam, pp 99–149
21. Tsierkezos NG, Szroeder P, Fuge R, Ritter U (2015) Electrochemical studies on novel films consisting of phosphorus-doped multi-walled carbon nanotubes. Ionics 21:1081
22. Solak AO, Eichorst LR, Clark WJ, McCreery RL (2003) Modified carbon surfaces as organic electrodes that exhibit conductance switching. Anal Chem 75:296
23. Nicholson RS, Shain I (1964) Theory of stationary electrode polarography single scan and cyclic methods applied to reversible, irreversible, and kinetic systems. Anal Chem 36:706
24. Min YS, Bae EJ, Kim UJ, Lee EH, Park N, Hwang CS, Park W (2008) Unusual transport characteristics of nitrogen-doped single-walled carbon nanotubes. Appl Phys Lett 93:043113
25. Perenlei G, Tee TW, Yusof NA, Kheng GJ (2011) Voltammetric detection of dotassium ferricyanide mediated by multi-walled carbon nanotube/titanium dioxide composite modified glassy carbon electrode. Int J Electrochem Sci 6:520
26. Pandurangachar M, Swamy BEK, Chandrashekar BN, Gilbert O, Reddy S, Sherigara BS (2010) Electrochemical investigations of potassium ferricyanide and dopamine by 1-butyl-4-methylpyridinium tetrafluoro borate modified carbon paste electrode: a cyclic voltammetric study. Int J Electrochem Sci 5:1187
27. Niranjana E, Swamy BEK, Naik RR, Sherigara BS, Jayadevappa H (2009) Electrochemical investigations of potassium ferricyanide and dopamine by sodium dodecyl sulphate modified carbon paste electrode: a cyclic voltammetric study. J Electroanal Chem 631:1
28. Hirano A, Kanai M, Nara T, Sugawara M (2001) A glass capillary ultramicroelectrode with an electrokinetic sampling ability. Anal Sci 17:37
29. Climent MA, Rodes A, Valls MJ, Peres JM, Fellu JM, Aldaz A (1994) Voltammetric and subtractively normalized interfacial FTIR study of the adsorption and oxidation of L(+)-ascorbic acid on Pt electrodes in acid medium: effect of Bi adatoms. J Chem Soc Faraday Trans 90:609
30. Tsierkezos NG, Ritter U (2012) Simultaneous detection of ascorbic acid and uric acid at MWCNT modified electrodes. J Nanosci Lett 2:25
31. Tsierkezos NG, Ritter U, Nugraha Thaha Y, Downing C, Szroeder P (2015) Synthesis, characterization, and electrochemical application of phosphorus-doped multi-walled carbon nanotubes. J Solid State Electrochem 19:891
32. Razmi H, Agazadeh M, Habibi B (2003) Electrocatalytic oxidation of dopamine at aluminum electrode modified with nickel pentacyanonitrosylferrate films, synthesized by electroless procedure. J Electroanal Chem 547:25
33. Owens JL, Marsh HA, Dryhurst G (1978) Electrochemical oxidation of uric acid and xanthine: an investigation by cyclic voltammetry, double potential step chronoamperometry and thin-layer spectroelectrochemistry. J Electroanal Chem 91:231
34. Tsierkezos NG, Ritter R (2012) Oxidation of dopamine on multi-walled carbon nanotubes. J Solid State Electrochem 16:2217
35. Kamyabi MA, Narimani O, Monfared HH (2011) Electroless deposition of bis(4′-(4-pyridyl)-2,2′:6′,2″-terpyridine)iron(II) thiocyanate complex onto carbon nanotubes modified glassy carbon electrode: application to simultaneous determination of ascorbic acid, dopamine and uric acid. J Braz Chem Soc 22:468